PAPER

Diketopyrrolopyrrole-based acceptors with multi-arms for organic solar cells†

Po Sun,[abc] Xiangzhi Li,[ab] Yulong Wang,[b] Haiquan Shan,[b] Jiaju Xu,[b] Changmei Liu,[a] Cong Zhang,[a] Fei Chen,[a] Zongxiang Xu, [iD] *[b] Zhi-kuan Chen [iD] *[a] and Wei Huang [iD] *[a]

Three small molecules **SBF-1DPPDCV**, **SBF-2DPPDCV** and **SBF-4DPPDCV** consisting of a spirobifluorene (SBF) unit as the core and one, two, and four diketopyrrolopyrrole dicyanovinyl (DPPDCV) units as the arms have been designed and synthesized for solution-processed bulk-heterojunction (BHJ) solar cells. The UV-Vis absorption and cyclic voltammetry measurement of these compounds showed that all these compounds have an intense absorption band over 300–750 nm with a LUMO energy level at around −3.87 eV. When pairing with PTB7-Th as the donor, devices fabricated based on PTB7-Th : **SBF-4DPPDCV** blends showed a decent PCE of 3.85%, which is the highest power conversion efficiency (PCE) amongst the three DPP acceptor fabricated devices without extra treatment. Devices with **SBF-1DPPDCV** and **SBF-2DPPDCV** acceptors showed lower PCEs of 0.26% for **SBF-1DPPDCV** and 0.98% for **SBF-2DPPDCV** respectively. The three dimensional (3D) structure of **SBF-4DPPDCV** facilitates the formation of a 3D charge-transport network and thus enables a rational electron-transport ability (1.04×10^{-4} cm^2 V^{-1} s^{-1}), which further leads to a higher J_{sc} (10.71 mA cm^{-2}). These findings suggest that multi-arm acceptors present better performance than one-arm or two-arm molecules for organic solar cells.

1 Introduction

The last decade has witnessed rapid progress in solution processed bulk heterojunction organic photovoltaics (OPVs) boosted by the design and synthesis of novel donor materials, owing to their potential advantages such as low cost, light weight, and flexibility.[1–3] To date, a power conversion efficiency (PCE) of >10% has been achieved for fullerene-based OPVs.[4–8]

Fullerene-derivatives, such as PC$_{61}$BM and PC71BM, have been used to play a dominant role as electron acceptors in the OPV research community. The high electron mobility as well as the isotropic charge-transporting characteristics of fullerene-derivatives made them superior to organic acceptors. Despite the significant success of fullerene-derivative acceptors in OPVs, their further improvement is limited due to their poor light-harvesting capability for solar light, low chemical/energetic tailorability, and the tedious synthesis and purification process, especially for industrial scale applications. In the past years, some new non-fullerene acceptors that showed much better performance than fullerenes have been found.[9,10] The power conversion efficiency of fullerene-free OPVs using a polymer donor PBDB-T-2Cl paired with a small molecular acceptor IT-4F blend has surpassed 14% by far.[11]

Currently, non-fullerene acceptor materials, including small molecules and polymers, have strong electron deficient units such as naphthalene diimide (NDI),[12,13] perylene diimide (PDI),[14–16] diketopyrrolopyrrole (DPP),[17–20] or other building blocks with electron withdrawing moieties.[21–23] Small molecular acceptors are normally believed to be more superior than polymeric acceptors in terms of their purity and small batch to batch variance on synthesis, which is important for industrial scale applications.[24,25] However, most of the small molecule acceptors do not have 3D ball-shape molecular structure thus may not form a 3D charge-transporting network as readily as fullerenes do.[26–28] For these reasons, a potentially promising approach is to develop small molecular materials with quasi-3D or 3D molecular structures.[14] Zhan and co-workers have demonstrated a novel, nonplanar, star-shaped PDI acceptor S(TPA-PDI) with a triphenylamine (TPA) core, which exhibited a quasi-3D structure.[29] Yan's group designed a unique 3D molecular TPE-PDI4 with the highly twisted nature of the tetraphenylethylene (TPE) core, which gave a PCE of 5.53% for non-fullerene based OPVs.[14] Ma and Cho reported SBF-PDI4 consisting of SBF-core and tetra-PDI subunits that constructed a 3D geometry.[30,31] Chen's group synthesized a series of materials based on DPP, amongst of them SF-4DPP4 and SF-DPPB4 with spirobifluorene (SBF) core as acceptor materials showed good

[a] Key Laboratory of Flexible Electronics (KLOFE) & Institute of Advanced Materials (IAM), National Jiangsu Synergistic Innovation Center for Advanced Materials, Nanjing Tech University, 30 South Puzhu Road, Nanjing 211816, China. E-mail: iamzkchen@njtech.edu.cn; iamwhuang@njtech.edu.cn

[b] Department of Chemistry, South University of Science and Technology of China, Shenzhen, P. R. China. E-mail: xu.zx@sustc.edu.cn

[c] Analysis and Testing Central Facility, Engineering Research Institute, Anhui University of Technology, Maanshan 243002, P. R. China. E-mail: sunpoo@ahut.edu.cn

† Electronic supplementary information (ESI) available. See DOI: 10.1039/c8ra03792b

performance when blended with P3HT, the PCEs of them were 3.63% and 5.16% respectively after annealing.[17,32] All of the above mentioned molecules have been found to exhibit a 3D molecular structure, as well as weak intermolecular interactions and weak molecular aggregation in the solid films and can easily form smooth films.

Aiming in further proving the nature of 3D dendrimeric acceptors, we report three small molecules consisting of SBF core attached with various numbers of DPP derivatives as arms to identify the effect of the 3D structures on acceptor performance in solar cells. Herein, SBF with an orthogonal molecular structure offers these new acceptor materials a perfect 3D geometry.[17,33–35] DPP derivative was selected to build up the arms because of its great light-harvesting capability as well as the excellent charge carrier transport behavior.[33,36–39] To further lower the energy levels, strong electron accepting dicyanovinyl (DCV) group was incorporated as well.[40–44] Based on these considerations, **SBF-1DPPDCV** functionalized with one arm, **SBF-2DPPDCV** with two arms, and **SBF-4DPPDCV** with four arms were designed (Fig. 1),[14,41,45,46] respectively. PTB7-Th was used as the donor for device fabrication and evaluation of the three acceptor molecules. The performance of devices based on PTB7-Th : acceptor blends suggested that 4-armed molecule, **SBF-4DPPDCV**, exhibited more superior performance than the other two materials, and a PCE as high as 3.85% was obtained, which is the highest PCE amongst the devices using DPP based acceptors without additives and annealing treatment.[17,47]

2   Results and discussion

2.1   Synthesis and characterization

The synthetic routes of the materials studied in this work are illustrated in Scheme 1. We synthesized SBF-2B and SBF-4B as the cores, and the electron withdrawing DPP arms functionalized with DCV as end capping groups. Then **SBF-1DPPDCV**, **SBF-2DPPDCV** and **SBF-4DPPDCV** were synthesized by Suzuki coupling reaction between DPPDCV arms and SBF cores. The chemical structures and purities were fully characterized by ¹H
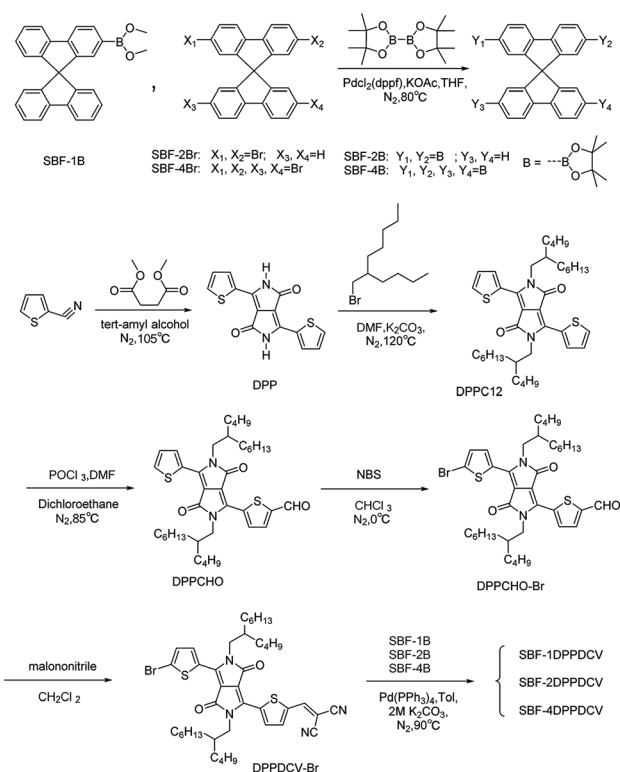
Scheme 1 Synthesis of SBF-1DPPDCV, SBF-2DPPDCV and SBF-4DPPDCV.

NMR, ^{13}C NMR (see Fig. S1–S12†), matrix-assisted laser desorption ionization time of flight (MALDI-TOF) mass spectroscopy (MS), and elemental analysis.

All of the molecules exhibited good solubility in common organic solvents such as chloroform and o-dichlorobenzene at room temperature because of the introduction of alkyl substituents to the primary structures.

2.2   Thermal properties

As shown in Fig. 2a, thermogravimetric analysis (TGA) under nitrogen indicates that decomposition temperatures (T_d, defined at the temperature at which 5% of the mass is lost) were 236 °C, 374 °C, and 383 °C for **SBF-1DPPDCV**, **SBF-2DPPDCV** and **SBF-4DPPDCV**, respectively. The higher T_d values observed for **SBF-2DPPDCV** and **SBF-4DPPDCV** indicated that the structures were more thermally stable.

The differential scanning calorimetry (DSC) analysis of the three compounds are illustrated in Fig. 2b. During the first
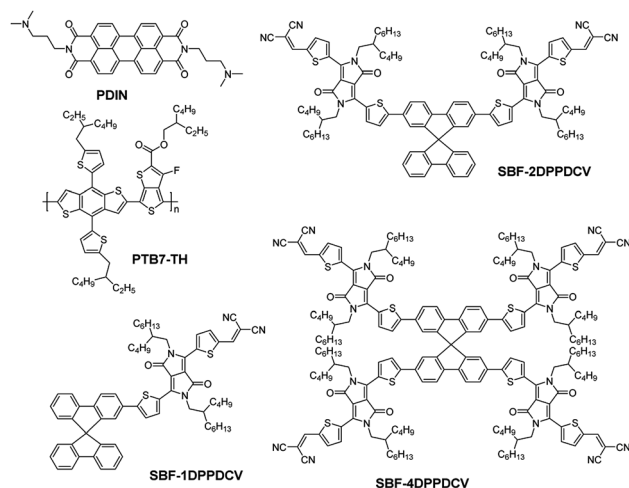
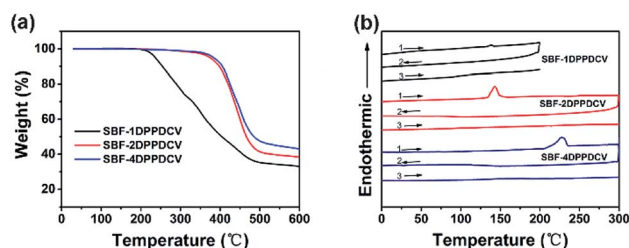**Fig. 1** Chemical structures of SBF-1DPPDCV, SBF-2DPPDCV, SBF-4DPPDCV, PTB7-Th and PDIN.

Fig. 2 (a) Thermogravimetric Analysis (TGA) and (b) Differential Scanning Calorimetry (DSC) of the compounds.

Table 1 Photophysical and electrochemical properties of the studied compounds

| Compounds | λ_{max} [nm] | | E_{onset}^{ox} [V] | E_{onset}^{red} [V] | HOMO [eV][a] | LUMO [eV][a] | Band gap [eV] |
	Solution	Film					
SBF-1DPPDCV	685	702	1.12	−0.51	−5.52	−3.89	1.59[b], 1.63[c]
SBF-2DPPDCV	700	717	1.06	−0.55	−5.46	−3.85	1.55[b], 1.61[c]
SBF-4DPPDCV	700	717	1.08	−0.54	−5.48	−3.86	1.56[b], 1.62[c]

[a] Calculated based on the respective onsets of oxidation and reduction potentials of the compounds *via* the equations: HOMO = −(E_{onset}^{ox} + 4.4) eV, LUMO = −(E_{onset}^{red} + 4.4) eV. [b] Based on the onset absorption data of thin films. [c] Based on the redox potentials.

heating scans, **SBF-1DPPDCV** showed weak melting peak at 138.5 °C, **SBF-2DPPDCV** and **SBF-4DPPDCV** exhibited sharp melting endothermic transitions at 143 °C and 227 °C respectively, which revealed certain degree of molecular order within the bulk materials. A broad shoulder peak was present in the onset of the melting curve for **SBF-4DPPDCV**, indicating the possible presence of conformational polymorphs.[9] While no obvious recrystallization was observed upon cooling and a featureless second heating was obtained, the materials then appeared to become kinetically trapped in the amorphous phase after melting, indicating a poorly crystalline property.[9,48]

2.3 Optical and electrochemical properties

Fig. 3a and b depicts the absorption spectra of three DPP acceptors in dichloromethane solutions and thin films. In solution, **SBF-1DPPDCV** exhibited absorption maxima at 685 nm with the extinction coefficient of 1.5×10^4 M^{-1} cm^{-1}, **SBF-2DPPDCV** and **SBF-4DPPDCV** exhibited absorption maxima at 700 nm with the extinction coefficients of 2.1×10^4 M^{-1} cm^{-1} and 1.4×10^5 M^{-1} cm^{-1}, respectively. The three compounds in dichloromethane solution exhibits similar absorption transition bands between 500–750 nm that can be ascribed to the intramolecular charge transfer (ICT) transitions between central SBF and terminal acceptor units.[49] The absorption

spectrum of **SBF-1DPPDCV** showed a peak value at ∼685 nm while those of **SBF-2DPPDCV** and **SBF-4DPPDCV** were at 700 nm. The slightly red shifted spectra of **SBF-2DPPDCV** and **SBF-4DPPDCV** compared with that of **SBF-1DPPDCV** is due to their larger π-conjugation on the DPP backbone. Similar profiles in the absorption spectra of **SBF-2DPPDCV** and **SBF-4DPPDCV** could be attributed to their similar chemical structure of the DPP and the limited electron coupling between the two perpendicular DPP in **SBF-4DPPDCV**.[50] Significant red-shifts in the absorption spectra were observed for all of the three acceptors in their thin-films compared with those in diluted solution, suggested the increase of molecular aggregation in the solid state. The optical bandgaps of **SBF-1DPPDCV**, **SBF-2DPPDCV** and **SBF-4DPPDCV** determined from the absorption onset of the absorption spectra of these compounds were estimated to be 1.59 eV, 1.55 eV and 1.56 eV, respectively (Table 1).

The electrochemical behaviors of the acceptor materials were investigated by cyclic voltammetry (CV) in anhydrous dichloromethane solutions, as shown in Fig. 3c. The lowest unoccupied molecular orbital (LUMO) and highest occupied molecular orbital (HOMO) of newly synthesized materials can be determined by their reduction and oxidation onset potentials respectively. The onset potentials were determined from the intersection of two tangents drawn as the rising current and baseline charging current of the CV traces. LUMO values were calculated (similar as HOMO value determination) from the corresponding reduction onsets using LUMO = −(E_{onset}^{red} + 4.4) eV. LUMO values were found to be −3.89 eV, −3.85 eV and −3.86 eV for **SBF-1DPPDCV**, **SBF-2DPPDCV**, and **SBF-4DPPDCV**, respectively (Table 1), which is close to $PC_{60}BM$ energy level. Moreover, similar to $PC_{60}BM$,[14,51] **SBF-4DPPDCV** exhibits 3D electron transportation characteristics. These acceptors show similar LUMO levels that can match well with the donor PTB7-Th and the interfacial material PDIN (Fig. 3d).

2.4 Theoretical calculations

The molecular geometry was optimized by density functional theory (DFT) using the B3LYP hybrid functional with basis set 6-31G(d). Quantum chemical calculation was performed with the Gaussian 09 package. In the calculations, the alkyl side chains of the molecules were replaced by methyl groups to reduce machine time. Fig. 4 illustrates the optimized ground-state geometries of the three acceptors. In the top view of three molecular, the two fluorene planes of the SBF-core were tilted at
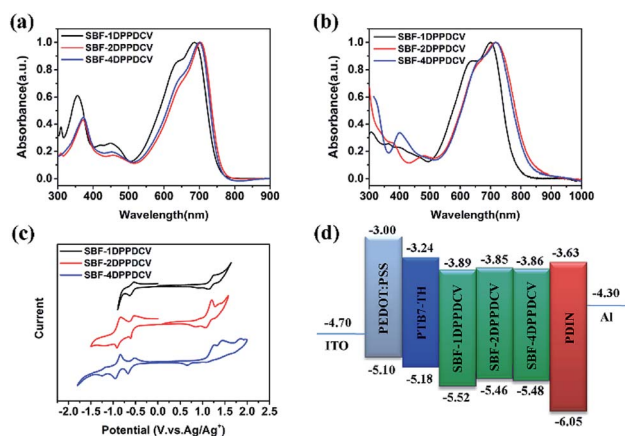

Fig. 3 (a) Normalized absorption spectra of the compounds in diluted dichloromethane and (b) normalized absorption spectra of thin films on glass; (c) cyclic voltammogram for the compounds in dichloromethane solution. (d) HOMO/LUMO energies for all compounds in the devices.
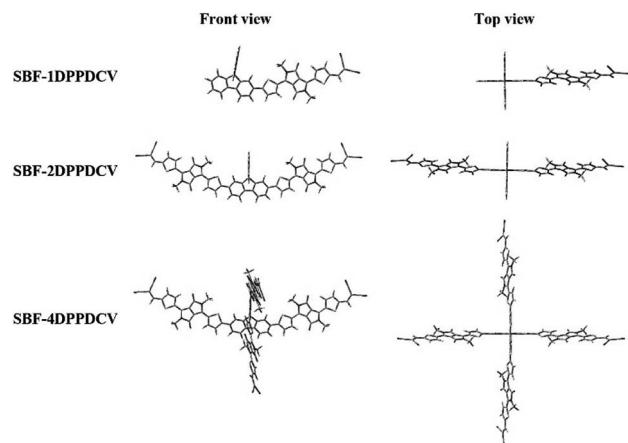
Fig. 4 Front and top views of **SBF-1DPPDCV**, **SBF-2DPPDCV** and **SBF-4DPPDCV** obtained by Tinker and optimized at B3LYP/6-31G(d) level.

an angle of 90°, so the four arms **SBF-4DPPDCV** tended to form a cross three-dimensional structure, while for **SBF-1DPPDCV** and **SBF-2DPPDCV**, the DPPDCV arms are only attached to one planar fluorene, and they does not form an obvious three-dimensional structure.

2.5 Device performances

The solution-processed BHJ solar cell devices were fabricated in a conventional configuration of ITO glass/PEDOT:PSS/PTB7-Th : acceptor/PDIN/Al and tested under an AM 1.5G simulated solar light at 100 mW cm^{-2}. Here, PEDOT:PSS and PDIN were used as hole transport layer and cathode interlayer respectively.[52] The blend films at a donor/acceptor weight ratio of 1.5 : 1 gave the best solar cell performance without additives and annealing treatment, as shown in Fig. 5a and Table 2. The device with **SBF-4DPPDCV** as acceptor afforded the best performance (V_{oc} = 0.74 V, J_{sc} = 10.71 mA cm^{-2}, FF = 48.69% and PCE = 3.85%). For the purpose of comparison, **SBF-1DPPDCV** and **SBF-2DPPDCV** under the same conditions gave

poorer photovoltaic performances with PCE of 0.98%, V_{oc} of 0.74 V, J_{sc} of 3.22 mA cm^{-2} and FF of 41.37% for **SBF-1DPPDCV**, and PCE of 0.26%, V_{oc} of 0.74 V, J_{sc} of 1.09 mA cm^{-2}, and FF of 31.52% for **SBF-2DPPDCV**, respectively. The three devices exhibited the same V_{oc} as the three acceptors showed similar LUMO energy levels. But the fill factor and short circuit current of **SBF-4DPPDCV** were much higher than **SBF-1DPPDCV** and **SBF-2DPPDCV**.

The external quantum efficiency (EQE) of the blended films with a PTB7-Th/acceptor weight ratio of 1.5 : 1 without any post-treatment is shown in Fig. 5b. All of the blended films showed broad EQE spectra in the range from 300 nm to 800 nm, with the EQE maximum peaks at 750 nm. While the peak intensity of spectra increases from 5% for **SBF-1DPPDCV** to 55% for **SBF-4DPPDCV**, which matched well with the increase of J_{sc}. Since the absorption spectra of PTB7-Th and DPP-based acceptors are very similar and have strong overlap in the region of 300 nm −800 nm, it was hard to differentiate their respective contributions to the photocurrent.

The electron and hole mobilities of the devices were estimated from space-charge-limited current (SCLC) measurements.[52] For hole-only and electron-only devices, the structures of ITO/PEDOT:PSS/PTB7-Th : acceptors (1.5 : 1, w/w)/Au and Al/PTB7-Th : acceptors (1.5 : 1, w/w)/Al were used, respectively (Fig. 5c and d). The estimated hole and electron mobilities are summarized in Table 2. The PTB7-Th : **SBF-1DPPDCV** blend films displayed a hole mobility (μ_h) and an electron mobility (μ_e) of 6.97×10^{-5} cm^2 V^{-1} s^{-1} and 6.14×10^{-6} cm^2 V^{-1} s^{-1}, respectively (μ_h/μ_e = 11.4). The PTB7-Th : **SBF-2DPPDCV** blend films exhibited a better balanced charge transport ($\mu_h = 1.04 \times 10^{-4}$ cm^2 V^{-1} s^{-1}, $\mu_e = 3.66 \times 10^{-5}$ cm^2 V^{-1} s^{-1}; μ_h/μ_e = 2.84). Among the three devices, PTB7-Th : **SBF-4DPPDCV** exhibits the highest and the most balanced charge mobility with μ_h of 1.06×10^{-4} cm^2 V^{-1} s^{-1}, μ_e of 1.04×10^{-4} cm^2 V^{-1} s^{-1}, μ_h/μ_e ratio of 1.01. It suggests that variation of the 3D conformation of the non-fullerene acceptor material does significantly tune the bulk charge transport properties of the BHJ devices, and the higher and more balanced charge transport is beneficial to J_{sc} and PCE enhancement.[10,19]

2.6 Film morphology

Fig. 6 shows the atomic force microscope (AFM) images of the blend thin films of PTB7-Th : acceptors at weight ratios of 1.5 : 1. The root-mean-square (RMS) roughness of the three compounds was found to be 1.66 nm, 1.41 nm and 1.10 nm for the blend films with **SBF-1DPPDCV**, **SBF-2DPPDCV**, and **SBF-4DPPDCV**, respectively. The films of PTB7-Th blended with **SBF-1DPPDCV** at a weight ratio of 1.5 : 1 produced a significantly larger domain size (60–80 nm). For **SBF-2DPPDCV**, AFM image shows a domain size between 30 nm and 40 nm, while it was ∼20–30 nm for **SBF-4DPPDCV** and continuous interpenetrating networks for charge transportation were formed, which could be the reason of the improvement of electron and hole mobilities. The continuous mesh structure induced by the 4-arm cross structures of SBF can be beneficial to efficient exciton dissociation and charge transportation in the thin films.
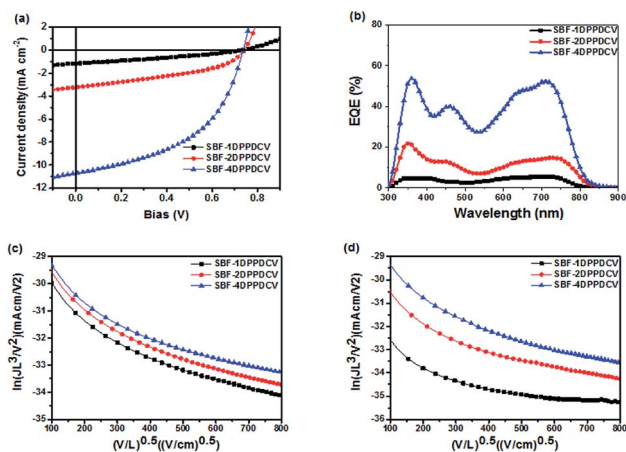

Fig. 5 (a) J−V curves of OPVs based on PTB7-Th : acceptors under the illumination of AM 1.5G, 100 mW cm^{-2}; (b) EQE spectra of PTB7-Th : acceptors PSCs; plots of ln(JL^3/V^2) vs. (V/L)$^{0.5}$ extracted from (c) ITO/PEDOT:PSS/PTB7-Th : acceptors/Au hole-only devices and (d) Al/PTB7-Th : acceptors/Al electron-only devices.

Table 2 The device data of OPVs based on PTB7-Th : acceptors under the illumination of AM 1.5G, 100 mW cm^{-2}

Donor : acceptor	w/w	V_{oc} [V]	J_{sc} [mA cm^{-2}]	FF [%]	PCE^a [%]	$\mu_h{}^b$ [cm^2 V^{-1} s^{-1}]	μ_e	μ_h/μ_e
PTB7-Th : **SBF-1DPPDCV**	1.5 : 1	0.74	1.09	31.52	0.26 (0.23)	6.97×10^{-5}	6.14×10^{-6}	11.4
PTB7-Th : **SBF-2DPPDCV**	1.5 : 1	0.74	3.22	41.37	0.98 (0.92)	1.04×10^{-4}	3.66×10^{-5}	2.84
PTB7-Th : **SBF-4DPPDCV**	1.5 : 1	0.74	10.71	48.69	**3.85 (3.79)**	1.06×10^{-4}	1.04×10^{-4}	1.01

^{a} The best and average (in brackets, over 12 devices) PCEs. ^{b} Hole and electron mobilities measured by SCLC method.

3 Experimental

3.1 General

Most of the organic and inorganic chemicals in this work were obtained from Aldrich, Alfa Aesar, and TCI and used without further purification. ^{1}H and ^{13}C NMR spectra were collected on a Bruker 400 MHz spectrometer. Chemical shifts for ^{1}H and ^{13}C NMR were referenced to residual signals from CDCl$_3$ (^{1}H NMR $\delta = 7.26$ ppm and ^{13}C NMR $\delta = 77.23$ ppm). Matrix-assisted laser desorption-ionization time of flight mass spectrometry (MALDI-TOF MS) was performed on a Bruker Autoflex II. Samples were prepared by diluting the molecules in CH$_2$Cl$_2$ using 2,5-dihydroxybenzoic acid as the matrix. Elemental analyses were conducted on a Flash EA 1112 elemental analyzer. Solution and thin-film UV-Vis absorption spectra were recorded on a UV-1750 UV-VIS spectrophotometer. Electrochemical measurements were carried out under nitrogen in deoxygenated 0.1 M solutions of tetra-n-butylammonium hexafluorophosphate in dry dichloromethane using a CHI 660E electrochemical workstation, a glassy-carbon working electrode, a platinum-wire auxiliary electrode, and an Ag wire anodised with AgCl as a pseudo-reference electrode. The cyclic voltammetry was performed using a scan rate of 100 mV s^{-1}. The potentials were referenced to Ag/AgCl by use of internal ferrocene. TGA measurements were performed on a TA Discovery TGA analyzer under nitrogen with a heating rate of 10 °C min^{-1}. DSC measurements were performed on a TA Discovery DSC analyzer under nitrogen with a heating rate of 10 °C min^{-1}. The surface morphologies of the thin films were examined using atomic force microscopy (AFM, MFP-3D Classic, tapping mode).

Fig. 6 AFM height (a, b and c) and phase (d, e and f) images of PTB7-Th blend with **SBF-1DPPDCV** (a and d), **SBF-2DPPDCV** (b and e) and **SBF-4DPPDCV** (c and f) at a weight ratio of 1.5 : 1. The scale bar in all images is 500 nm.

3.2 Synthesis

3.2.1 Synthesis of 2,2′,7,7′-tetrakis(4,4,5,5-tetramethyl-1,3,2-dioxaborolan-2-yl)-9,9′-spirobi[fluorene] (SBF-4B). A solution of 2,2′,7,7′-tetrabromo-9,9′-spirobi[fluorene] (1.60 g, 2.50 mmol), bis(pinacolato)diboron (3.80 g, 15.0 mmol), Pd(dppf)Cl$_2$ (0.40 g, 0.50 mmol), and KOAc (2.90 g, 30.0 mmol) in THF (150 mL) was stirred at 80 °C under N$_2$ for three days. The reaction was quenched by adding DI water, and the resulting mixture was washed with ethyl acetate (50 mL × 3). Then the organic layers were washed with brine, dried over with Na$_2$SO$_4$, and dried in vacuum box. After purification by silica gel column chromatography using CH$_2$Cl$_2$/hexane (v/v, 1/1), white solid was obtained in a yield of 79% (1.66 g). ^{1}H NMR (400 MHz, CDCl$_3$). δ (ppm) 7.87 (m, 8H), 7.08 (s, 4H), 1.23 (s, 48H). MALD-TOF MS: calcd for C$_{49}$H$_{60}$B$_4$O$_8$: 820.47, found 820.25.

3.2.2 Synthesis of 2,7-bis(4,4,5,5-tetramethyl-1,3,2-dioxaborolan-2-yl)-9,9′-spirobi[fluorene] (SBF-2B). The synthetic route of SBF-2B was similar to the synthesis of SBF-4B. White solids were obtained (yield 50%). ^{1}H NMR (400 MHz, CDCl$_3$). δ (ppm) 7.72 (m, 4H), 7.19 (m, 2H), 7.09 (s, 2H), 6.97 (s, 2H), 6.91 (m, 2H), 6.49 (d, $J = 7.4$, 2H), 0.96 (s, 24H). MALD-TOF MS: calcd for C$_{37}$H$_{38}$B$_2$O$_4$: 568.30, found 568.33.

3.2.3 Synthesis of 3,6-di(thiophen-2-yl)pyrrolo[3,4-c]pyrrole-1,4(2H, 5H)-dione (DPP). Potassium $tert$-butoxide (20.0 g, 180 mmol) was added to a round-bottom flask with argon protection. A solution of $tert$-amyl alcohol (125 mL) and 2-thiophenecarbonitrile (16.4 g, 150 mmol) was injected in one portion. The mixture was heated to 105 °C, and a solution of dimethyl succinate (7.30 g, 50.0 mmol) in t-amyl alcohol (40 mL) was introduced dropwise in 1 h. The reaction was stirred and heated at 105 °C for 1 h, and then the methanol byproduct was distilled off, and the reaction mixture was kept stirring at 105 °C for 2 h. The reaction mixture was then cooled down to 65 °C, diluted with 50 mL of methanol, neutralized with acetic acid, and refluxed for 10 min. The resulting suspension was filtered, and the black filter cake was washed with hot methanol and water twice, and then dried in vacuum box to afford a purple black solid in a yield of 88.2% (13.2 g).

3.2.4 Synthesis of 2,5-dibutyloctyl-3,6-dithiophen-2-ylpyrrolo[3,4-c]pyrrole-1,4-dione (DPP-C12). DPP (13.0 g, 43.3 mmol) and anhydrous potassium carbonate (24.0 g, 173 mmol) were dissolved in N,N-dimethylformamide (250 mL) in a two-necked round flask, and heated to 145 °C under argon protection. 2-Butyloctyl bromide (49.8 g, 200 mmol) was introduced in one portion by syringe. After stirring at 145 °C for 12 h, the solution was allowed to cool down to room temperature, and then 500 mL ice water was poured into. The suspension was filtered, and the solid collected on the filter paper was washed with water
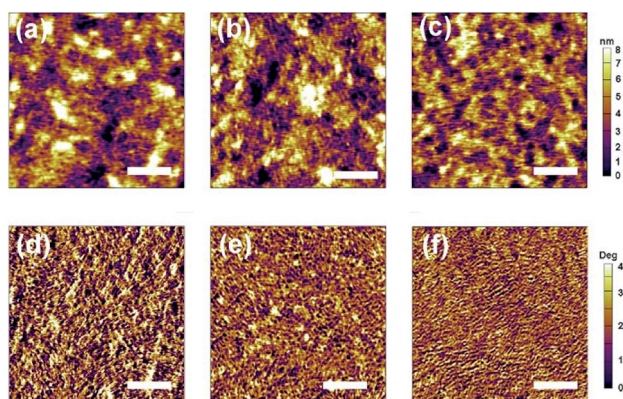
and methanol successively, and then dried in vacuum box. The crude product was purified by silica gel column chromatography using dichloromethane as eluent to give a deep purple solid (15.2 g, yield 67%). ^{1}H NMR (400 MHz, CDCl$_3$): δ (ppm) 8.86 (d, J = 3.4 Hz, 2H), 7.63 (d, J = 4.8 Hz, 2H), 7.28 (s, 2H), 4.03 (d, J = 7.6 Hz, 4H), 1.91 (m, 2H), 1.43–1.25 (m, 32H), 0.84 (m, 12H). MALD-TOF MS: calcd for $C_{38}H_{56}N_2O_2S_2$: 634.40, found 635.32.

3.2.5 Synthesis of 5-(2,5-bis(2-butyloctyl)-3,6-dioxo-4-(thiophen-2-yl)-2,3,5,6-tetrahydropyrrolo[3,4-c]pyrrol-1-yl)thiophene-2-carbaldehyde (DPPCHO).

POCl3 (7.66 g, 50.0 mmol) was added dropwise into a mixture of N,N-dimethylformamide (3.65 g, 50.0 mmol) and 1,2-dichloroethane (5 mL) at 0 °C. The mixture was stirred at room temperature until the orange Vilsmeier reagent was obtained. The above Vilsmeier reagent was added dropwise into the solution of 3,6-di(thiophen-2-yl)pyrrolo[3,4-c]pyrrole-1,4(2H,5H)-Dione (DPP-C12) (1.85 g, 2.90 mmol) in 1,2-dichloroethane (50 mL). The mixture was stirred and heated at 85 °C for overnight, and then cooled down to room temperature. After the introduction of a saturated NaHCO$_3$ aqueous solution, the mixture was kept stirring for 2 h. The product was extracted with CH$_2$Cl$_2$ (20 mL × 3), and the organic components were collected and washed successively with DI water and brine, and then dried over MgSO$_4$. The crude product was purified by silica gel column chromatography using CH$_2$Cl$_2$/petroleum ether (v/v, 1/1) as eluent to afford the purple solid in a yield of 47.5% (0.91 g). ^{1}H NMR (400 MHz, CDCl$_3$): δ (ppm) 10.03 (s, 1H), 9.04 (dd, J = 3.9, 1.1 Hz, 1H), 8.92 (d, J = 4.2 Hz, 1H), 7.87 (d, J = 4.2 Hz, 1H), 7.73 (dd, J = 5.0, 1.1 Hz, 1H), 7.33 (dd, J = 5.0, 4.0 Hz, 1H), 4.07 (m, 4H), 1.85–1.95 (m, 2H), 1.2–1.4 (m, 32H), 0.8–1.0 (m, 12H). MALD-TOF MS: calcd for $C_{39}H_{56}N_2O_3S_2$: 664.37, found 663.13.

3.2.6 Synthesis of 5-(4-(5-bromothiophen-2-yl)-2,5-bis(2-butyloctyl)-3,6-dioxo-2,3,5,6-tetrahydropyrrolo[3,4-c]pyrrol-1-yl)thiophene-2-carbaldehyde (DPPCHO-Br).

A solution of N-bromosuccinimide (NBS) (0.15 g, 0.86 mmol) in CHCl$_3$ (30 mL) was added dropwise into a solution of 5-(2,5-bis(2-butyloctyl)-3,6-dioxo-4- (thiophen-2-yl)-2,3,5,6-tetrahydropyrrolo[3,4-c]pyrrol-1-yl)thiophene-2-carbaldehyde (DPPCHO) (0.57 g, 0.86 mmol) in CHCl$_3$ (30 mL) with stirring at 0 °C. The mixture was kept stirring at 0 °C for overnight and then quenched with 20 mL DI water. The aqueous phase was collected and extracted with CH$_2$Cl$_2$ (20 mL ×3). The combined organic phase was washed with brine, and then dried over anhydrous Na$_2$SO$_4$. After removal of the solvent under reduced pressure, the residue was purified by silica gel column chromatography using CH$_2$Cl$_2$/petroleum ether (v/v, 2/1) as eluent to afford purple red solid (331 mg, 52%). ^{1}H NMR (400 MHz, CDCl$_3$): δ (ppm) 10.03 (s, 1H), 9.03 (d, J = 4.7, 1H), 8.92 (d, J = 4.1 Hz, 1H), 7.87 (d, J = 4.2 Hz, 1H), 7.73 (d, J = 5.9 Hz, 1H), 7.33 (m, 1H), 4.06 (m, 4H), 1.85–2.00 (m, 2H), 1.2–1.4 (m, 32H), 0.8–1.0 (m, 12H). MALD-TOF MS: calcd for $C_{39}H_{55}BrN_2O_3S_2$: 742.28, found 742.13.

3.2.7 Synthesis of 2-((5-(4-(5-bromothiophen-2-yl)-2,5-bis(2-butyloctyl)-3,6-dioxo-2,3,5,6-tetrahydropyrrolo[3,4-c]pyrrol-1-yl)thiophen-2-yl)methylene)malononitrile (DPPDCV-Br).

A mixture of DPPCHO-Br (0.74 g, 1.00 mmol), malononitrile (0.26 g, 3.98 mmol), and aluminum oxide (0.77 g, 9.30 mmol), and CH$_2$Cl$_2$ (60 mL) was put in a 250 mL two-necked round bottom flask, and stirred at room temperature for 1 h. The resulting mixture was filtered, and residual solvent was removed by rotary evaporation. The crude product was dissolved in 2 mL CH$_2$Cl$_2$ and reprecipitated in methanol. The resulting suspension was filtered and dried in vacuum box to gave a dark blue solid powder. Yield: 69.62% (0.55 g). ^{1}H NMR (400 MHz, CDCl$_3$): δ(ppm) 9.02 (d, J = 4.3 Hz, 1H), 8.84 (d, J = 4.2, 1H), 7.87 (s, 1H), 7.80 (d, J = 4.3, 1H), 7.26 (d, J = 3.9, 1H), 3.98 (dd, J = 33.6, 7.3 Hz, 4H), 1.85–1.95 (m, 2H), 1.2–1.4 (m, 32H), 0.8–1.0 (m, 12H). MALD-TOF MS: calcd for $C_{42}H_{55}BrN_4O_2S_2$: 790.29, found 790.05.

3.2.8 Synthesis of SBF-4DPPDCV.

A mixture of SBF-4B (82.0 mg, 0.10 mmol), DPPDCV-Br (396 mg, 0.50 mmol), aqueous 2 M K$_2$CO$_3$ (2.5 mL, 5.00 mmol), Aliquat 336 (1 drop), and toluene (8 mL) was carefully degassed for 20 min before and after the addition of Pd(PPh$_3$)$_4$ (47.0 mg, 0.04 mmol). Then the resulting mixture was heated to 85 °C and stirred under a nitrogen atmosphere for 36 h. After cooling down to room temperature, water and CH$_2$Cl$_2$ were added, the organic layer was separated, the aqueous layer was extracted with CH$_2$Cl$_2$, and the combined organic layers were dried over anhydrous Na$_2$SO$_4$. After removal of the solvent under reduced pressure, the residue was purified by column chromatography on silica gel using CH$_2$Cl$_2$/petroleum ether (v/v, 1/3) as eluent to afford a purple black solid (113 mg, 36%). ^{1}H NMR (400 MHz, CDCl$_3$): δ(ppm) 9.00 (m, 4H), 8.06 (d, J = 8.0 Hz, 4H), 7.86 (d, J = 8.2 Hz, 4H), 7.80 (s, 4H), 7.75 (d, J = 4.2 Hz, 4H), 7.39 (d, J = 4.0 Hz, 4H), 7.35–7.27 (m, 4H), 7.16 (s, 4H), 4.02 (s, 16H), 1.95–1.80 (m, 8H), 1.40–1.10 (m, 128H), 1.00–0.50 (m, 48H). ^{13}C NMR (100 MHz, CDCl$_3$): δ(ppm) 161.80, 160.92, 151.42, 149.39, 149.19, 142.82, 142.05, 139.04, 138.48, 137.56, 136.15, 134.67, 133.40, 132.55, 130.52, 128.43, 127.71, 125.32, 121.61, 121.49, 113.87, 113.11, 112.37, 108.78, 78.84, 46.62, 46.49, 38.36, 37.89, 32.97, 31.71, 31.69, 31.13, 30.88, 30.60, 29.73, 29.62, 28.38, 28.23, 26.13, 26.03, 24.83, 23.02, 22.99, 22.61, 14.19, 14.16, 14.12, 14.07. MALDI-TOF-MS: calcd for $C_{193}H_{232}N_{16}O_8S_8$: 3157.60; Found: 3159.03. Elemental analysis calcd for $C_{193}H_{232}N_{16}O_8S_8$: C 73.35, H 7.40, N 7.09%; found C 72.92, H 7.44, N 6.70%.

3.2.9 Synthesis of SBF-1DPPDCV and SBF-2DPPDCV.

The synthetic route of SBF-1DPPDCV and SBF-2DPPDCV was similar to the synthesis of SBF-4DPPDCV. And they were purified by silica gel chromatography (petroleum ether:CH$_2$Cl$_2$ = 1 : 1 for SBF-1DPPDCV and 1 : 3 for SBF-2DPPDCV, respectively).

SBF-1DPPDCV (black solid, yield 50%). ^{1}H NMR (400 MHz, CDCl$_3$): δ(ppm) 9.01 (m, 2H), 7.88 (m, 4H), 7.82 (s, 1H), 7.79 (d, J = 4.1 Hz, 1H), 7.71 (d, J = 8.0 Hz, 1H), 7.40 (m, 3H), 7.30 (d, J = 4.4 Hz, 1H), 7.14 (m, 3H), 7.03 (s, 1H), 6.81–6.70 (m, 3H), 4.02 (m, 4H), 1.95–1.80 (m, 2H), 1.40–1.10 (m, 32H), 1.00–0.50 (m, 12H). ^{13}C NMR (100 MHz, CDCl$_3$): δ(ppm) 162.27, 160.04, 152.21, 149.75, 149.09, 149.01, 147.86, 143.99, 143.17, 143.14, 141.59, 140.22, 140.05, 138.76, 138.56, 136.03, 134.51, 134.46, 134.41, 133.13, 132.45, 130.41, 130.16, 129.96, 128.16, 128.12, 128.08, 127.99, 127.96, 126.43, 124.97, 124.04, 121.59, 120.74, 120.35, 120.19, 114.21, 113.44, 113.20, 113.11, 108.49, 104.22, 78.49, 46.31, 45.96, 38.31, 37.44, 31.83, 31.68, 31.02, 30.77, 30.61, 29.92, 29.72, 29.61, 28.30, 26.09, 24.80, 23.23, 23.10,

22.81, 14.36, 14.32, 14.24, 14.18. MALDI-TOF-MS: calcd for $C_{67}H_{70}N_4O_2S_2$: 1027.44; found: 1026.78. Elemental analysis calcd for $C_{67}H_{70}N_4O_2S_2$: C 78.32, H 6.87, N 5.45%; found C 77.74, H 6.96, N 5.38%.

SBF-2DPPDCV *(black solid, yield 40%)*. ^{1}H NMR (400 MHz, CDCl$_3$): δ(ppm) 9.01 (dd, J = 6.6, 4.3 Hz, 4H), 7.94 (d, J = 2.9 Hz, 2H), 7.92 (d, J = 3.1 Hz, 2H), 7.83 (s, 1H), 7.78 (d, J = 4.4 Hz, 2H), 7.74 (dd, J = 8.0, 1.7 Hz, 2H), 7.45 (t, J = 7.5 Hz, 2H), 7.33 (d, J = 4.2 Hz, 2H), 7.17 (t, J = 7.5 Hz, 2H), 7.01 (s, 2H), 6.82 (d, J = 7.2 Hz, 2H), 4.02 (dd, J = 13.1, 7.8 Hz, 8H), 1.87 (m, 4H), 1.40–1.10 (m, 64H), 0.90–0.75 (m, 24H). ^{13}C NMR (100 MHz, CDCl$_3$): δ(ppm) 161.85, 160.89, 151.85, 150.62, 149.21, 147.42, 146.32, 143.16, 142.02, 141.84, 139.24, 138.89, 138.55, 137.46, 135.98, 134.60, 133.05, 128.34, 128.20, 126.66, 125.24, 124.06, 121.56, 121.54, 120.46, 113.84, 113.06, 112.44, 108.60, 78.72, 46.55, 46.42, 38.30, 37.76, 31.72, 31.08, 30.90, 30.83, 30.63, 29.63, 28.34, 28.26, 26.10, 26.06, 23.04, 22.98, 22.62, 14.10, 14.09, 14.04, 14.00. MALDI-TOF-MS: calcd for $C_{109}H_{124}N_8O_4S_4$: 1736.86; found: 1738.04 (M + 1). Elemental analysis calcd for $C_{109}H_{124}N_8O_4S_4$: C 75.31, H 7.19, N 6.45%; found C 75.12, H 7.28, N 6.16%.

3.3 Photovoltaic cells

OSCs were fabricated with the structure ITO/PEDOT: PSS/PTB7-Th : acceptors/PDIN/Al. The patterned ITO glass was precleaned in an ultrasonic bath of acetone and isopropyl alcohol, and treated in an ultraviolet-ozone chamber (Novascan Company, USA) for 20 min. A thin layer (30 nm) of PEDOT:PSS (Baytron P, now Clevios VP AI 4083, from H. C. Starck, Leverkusen, Germany) was spin-coated onto the ITO glass and baked at 150 °C for 15 min. A solution (total of 30 mg mL^{-1}) of PTB7-Th : acceptors blend was subsequently spin-coated (2000 rpm) on the PEDOT:PSS layer to form a photosensitive layer (*ca.*100 nm thick). The thickness of the photosensitive layer was measured using an Ambios Technology (Santa Cruz, CA) XP-2 profilometer. The methanol solution (0.2% acetic acid) of PDIN at a concentration of 1.5 mg mL^{-1} was deposited on the active layer at 3000 rpm for 30 s, giving a PDIN layer *ca.* 13 nm thick. An aluminium (*ca.* 100 nm) layer was subsequently evaporated onto the surface of the PDIN layer under vacuum (*ca.* 10^{-6} Pa) to form the negative electrode. The active area of the device was 0.1 cm^2. The J–V curve was measured with a computer controlled Keithley 236 Source Measure Unit (Zolix ss150 Solar Simulator). A xenon lamp coupled with AM1.5 solar spectrum filters was used as the light source, and the optical power at the sample was 100 mW cm^{-2}. The light intensity of the solar simulator was calibrated using a standard silicon solar cell. The EQE spectrum was measured using a Solar Cell QE/EQE Measurement System (Zolix Solar cell scan 100) consisting of a model SR830 DSP lock-in amplifier coupled with a WDG3 monochromator and 500 W xenon lamp.

3.4 SCLC measurement: current–voltage (J–V)

Characteristics of the SCLC devices were measured by using a HP4155A semiconductor parameter analyzer (Yokogawa Hewlett-Packard, Tokyo). The carrier mobility was extracted by fitting the J-V curves in the near quadratic regions according to the modified Mott–Gurney equation:[53]

$$J = \frac{9}{8}\varepsilon\varepsilon_0\mu\frac{V^2}{L^3}\left(0.89\beta\frac{\sqrt{V}}{\sqrt{L}}\right) \tag{1}$$

where J is the current density, ε_0 is the permittivity of free space, ε is the relative permittivity, μ is the zero-field mobility, V is the applied voltage, L is the thickness of active layer, and β is the field-activation factor.

4 Conclusions

In summary, three conjugated molecules consisting of a spirobifluorene (SBF) core attached with different numbers of DPP arms were designed and synthesized, and utilized as nonfullerene acceptors for OPVs. The blend thin films of **SBF-4DPPDCV** with PTB7-Th as the donor at a weight ratio of 1.5 : 1 yielded the highest PCE of 3.85%, while the PCEs of **SBF-1DPPDCV** and **SBF-2DPPDCV** devices achieved PCEs of only 0.26% and 0.98% respectively. The superior performance of **SBF-4DPPDCV** to the others could be attributed to the multiple electronic transmission property of the materials as well as better phase separation morphology with a continuous mesh structure in the thin films blended with PTB7-Th.

Conflicts of interest

There are no conflicts to declare.

Acknowledgements

References

1 G. Yu, J. Gao, J. C Hummelen, F. Wudl and A. J. Heeger, Polymer Photovoltaic Cells: Enhanced Efficiencies *via* a Network of Internal Donor-Acceptor Heterojunctions, *Science*, 1995, **270**, 1789–1791.

2 Y. Cheng, S. Yang and C. Hsu, Synthesis of conjugated polymers for organic solar cell applications, *Chem. Rev.*, 2009, **109**, 5868–5923.

3 G. Li, R. Zhu and Y. Yang, Polymer solar cells, *Nat. Photonics*, 2012, **6**, 153–161.

4 B. Kan, Q. Zhang, M. Li, X. Wan, W. Ni, L. Guankui, Y. Wang, X. Yang, H. Feng and Y. Chen, Solution-Processed Organic Solar Cells Based on Dialkylthiol-Substituted Benzodithiophene Unit with Efficiency near 10%, *J. Am. Chem. Soc.*, 2014, **136**, 15529–15532.

5 Z. He, C. Zhong, S. Su, M. Xu, H. Wu and Y. Cao, Enhanced power conversion efficiency in polymer solar cells using an inverted device structure, *Nat. Photonics*, 2012, **6**, 593–597.

6 Y. Li, Over 10% efficiencies achieved for the PSCs with thick active layer based on D-A copolymer donors and various fullerene acceptors, *Sci. China: Chem.*, 2015, **58**, 188.

7 Y. Liu, J. Zhao, Z. Li, C. Mu, W. Ma, H. Hu, K. Jiang, H. Lin, H. Ade and H. Yan, Aggregation and morphology control enables multiple cases of high-efficiency polymer solar cells, *Nat. Commun.*, 2014, **5**, 5293.

8 J. D. Chen, C. Cui, Y. Q Li, L. Zhou, Q. D. Ou, C. Li, Y. Li and J. X. Tang, Single-Junction Polymer Solar Cells Exceeding 10% Power Conversion Efficiency, *Adv. Mater.*, 2015, **27**, 1035–1041.

9 J. Hou, O. Inganäs, R. H. Friend and F. Gao, Organic solar cells based on non-fullerene acceptors, *Nat. Mater.*, 2018, **17**, 119–128.

10 C. L. Zhan, X. L. Zhang and J. N. Yao, New advances in non-fullerene acceptor based organic solar cells, *RSC Adv.*, 2015, **5**, 93002–93026.

11 S. Q. Zhang, Y. P. Qin, J. Zhu and J. H. Hou, Over 14% Efficiency in Polymer Solar Cells Enabled by a Chlorinated Polymer Donor, *Adv. Mater.*, 2018, **18**, 868–875.

12 Y. Hwang, T. Earmme, B. A. E. Courtright, F. N. Eberle and S. A. Jenekhe, n-Type Semiconducting Naphthalene Diimide-Perylene Diimide Copolymers: Controlling Crystallinity, Blend Morphology, and Compatibility Toward High-Performance All-Polymer Solar Cells, *J. Am. Chem. Soc.*, 2015, **137**, 4424–4434.

13 J. W. Jung, J. W. Jo, C. C. Chueh, F. Liu, W. H. Jo, T. P. Russell and A. K. Y. Jen, Fluoro-Substituted n-Type Conjugated Polymers for Additive-Free All-Polymer Bulk Heterojunction Solar Cells with High Power Conversion Efficiency of 6.71, *Adv. Mater.*, 2015, **27**, 3310–3317.

14 Y. Liu, C. Mu, K. Jiang, J. Zhao, Y. Li, L. Zhang, Z. Li, J. Y. L. Lai, H. Hu, T. Ma, R. Hu, D. Yu, X. Huang, B. Z. Tang and H. Yan, A Tetraphenylethylene Core-Based 3D Structure Small Molecular Acceptor Enabling Efficient Non-Fullerene Organic Solar Cells, *Adv. Mater.*, 2015, **27**, 1015–1020.

15 H. Sun, P. Sun, C. Zhang, Y. G. Yang, X. Y. Gao, F. Chen, Z. X. Xu, Z. K. Chen and W. Huang, High Performance Organic Solar Cells Based on Non-Fullerene Acceptor with a Spiro Core, *Chem.–Asian J.*, 2017, **12**, 721–725.

16 Y. Zhao, H. Wang, S. P. Xia, F. Zhou, Z. H. Luo, J. J. Luo, F. He and C. L. Yang, 9,9′-Bifluorenylidene-Core Perylene Diimide Acceptors for As-Cast Non-Fullerene Organic Solar Cells: The Isomeric Effect on Optoelectronic Properties, *Chem.–Eur. J.*, 2018, **24**, 4149–4156.

17 P. Sun, H. Sun, X. Z Li, Y. L. Wang, H. Q. Shan, J. J. Xu, C. Zhang, Z. X. Xu, Z. K. Chen and W. Huang, Three dimensional multi-arm acceptors based on diketopyrrolopyrrole with (hetero)aromatic cores for non-fullerene organic solar cells without additional treatment, *Dyes Pigm.*, 2017, **139**, 412–419.

18 X. Wu, W. Fu, Z. Xu, M. Shi, F. Liu, H. Chen, J. Wan and T. P. Russell, Spiro Linkage as an Alternative Strategy for Promising Nonfullerene Acceptors in Organic Solar Cells, *Adv. Funct. Mater.*, 2015, **25**, 5954–5966.

19 H. Bai, P. Cheng, Y. Wang, L. Ma, Y. Li, D. Zhu and X. Zhan, A bipolar small molecule based on indacenodithiophene and diketopyrrolopyrrole for solution processed organic solar cells, *J. Mater. Chem. A*, 2014, **2**, 778–784.

20 W. Li, W. S. C. Roelofs, M. Turbiez, W. M. Martijn and R. A. J. Janssen, Polymer solar cells with diketopyrrolopyrrole conjugated polymers as the electron donor and electron acceptor, *Adv. Mater.*, 2014, **26**, 3304–3309.

21 Z. E. Ooi, T. T. Lip, S. R. Y. Cheong, Z. K. Chen, K. Thomas, S. Alan, B. Martin, M. Klaus and D. C. John, Solution processable bulk-heterojunction solar cells using a small molecule acceptor, *J. Mater. Chem.*, 2008, **18**, 4619–4622.

22 P. Sonar, G. M. Ng, T. T. Lin, A. Dodabalapur and Z. K. Chen, Solution processable low bandgap diketopyrrolopyrrole (DPP) based derivatives: novel acceptors for organic solar cells, *J. Mater. Chem.*, 2010, **20**, 3626–3636.

23 J. H. Miao, B. Meng, J. Liu and L. X. Wang, An A-D-A′-D-A type small molecule acceptor with a broad absorption spectrum for organic solar cells, *Chem. Commun.*, 2018, **54**, 303–306.

24 Kwon, J. H. Park and S. Y. Park, An efficient nonfullerene acceptor for all-small-molecule solar cells with versatile processability in environmentally benign solvents, *Org. Electron.*, 2016, **30**, 105–111.

25 J. M. Topple, S. M. Mcafee, G. C. Welch and I. G. Hill, Pivotal factors in solution-processed, non-fullerene, all small-molecule organic solar cell device optimization, *Org. Electron.*, 2015, **27**, 197–201.

26 M. Li, L. Wang, J. Liu, K. Zhou, X. Yu, R. Xing, Y. Geng and Y. Han, Cooperative effects of solvent and polymer acceptor co-additives in P3HT: PDI solar cells: simultaneous optimization in lateral and vertical phase separation, *Phys. Chem. Chem. Phys.*, 2014, **16**, 4528–4537.

27 Howard, F. Laquai, P. E. Keivanidis, R. H. Friend and N. Greenham, Perylene Tetracarboxydiimide as an Electron Acceptor in Organic Solar Cells: A Study of Charge Generation and Recombination, *J. Phys. Chem. C*, 2009, **113**, 21225–21232.

28 V. Kamm, G. Battagliarin, I. A. Howard, W. Pisula, A. Mavrinskiy, C. Li, K. Müllen and F. Laquai, Polythiophene: Perylene Diimide Solar Cells-the Impact of Alkyl-Substitution on the Photovoltaic Performance, *Adv. Energy Mater.*, 2011, **1**, 297–302.

29 Y. Lin, Y. Wang, J. Wang, J. Hou, Y. Li, D. Zhu and X. Zhan, A star-shaped perylene diimide electron acceptor for high-performance organic solar cells, *Adv. Mater.*, 2014, **26**, 5137–5142.

30 J. Yi, Y. Wang, Q. Luo, Y. Lin, H. Tan, H. Wang and C. Q. Ma, A 9,9′-spirobi[9H-fluorene]-cored perylenediimide derivative and its application in organic solar cells as a non-fullerene acceptor, *Chem. Commun.*, 2015, **52**, 1649–1652.

31 J. Lee, R. Singh, D. H. Sin, H. G. Kim, K. C. Song and K. Cho, A Nonfullerene Small Molecule Acceptor with 3D Interlocking Geometry Enabling Efficient Organic Solar Cells, *Adv. Mater.*, 2015, **28**, 69–76.

32 S. Li, W. Liu, M. Shi, J. Mai, T. Lau, J. Wan, X. Lu, C. Li and H. Z. Chen, A spirobifluorene and diketopyrrolopyrrole moieties based non-fullerene acceptor for efficient and thermally stable polymer solar cells with high open-circuit voltage, *Energy Environ. Sci.*, 2015, **9**, 1649–1652.

33 Y. Qiao, Y. Guo, C. Yu, F. Zhang, W. Xu, Y. Liu and D. Zhu, Diketopyrrolopyrrole-containing quinoidal small molecules for high-performance, air-stable, and solution-processable n-channel organic field-effect transistors, *J. Am. Chem. Soc.*, 2012, **134**, 4084–4087.

34 J. Zhao, Y. Li, H. Lin, Y. Liu, K. Jiang, C. Mu, T. Ma, J. Y. L. Lai, H. Hu and D. Yu, High-efficiency non-fullerene organic solar cells enabled by a difluorobenzothiadiazole-based donor polymer combined with a properly matched small molecule acceptor, *Energy Environ. Sci.*, 2015, **8**, 520–525.

35 S. Ma, Y. Fu, D. Ni, J. Mao, Z. Xie and G. Tu, Spiro-fluorene based 3D donor towards efficient organic photovoltaics, *Chem. Commun.*, 2012, **48**, 11847–11849.

36 Y. Lin, P. Cheng, Y. Li and X. Zhan, A 3D star-shaped non-fullerene acceptor for solution-processed organic solar cells with a high open-circuit voltage of 1.18 V, *Chem. Commun.*, 2012, **48**, 4773–4775.

37 M. Shi, D. Deng, L. Chen, J. Ling, L. Fu, X. L. Hu and H. Z. Chen, Design and synthesis of dithieno[3,2-b:2′3′-d]pyrrole-based conjugated polymers for photovoltaic applications: consensus between low bandgap and low HOMO energy level, *J. Polym. Sci., Part A: Polym. Chem.*, 2011, **49**, 1453–1461.

38 J. Lee, A. R. Han, H. Yu, T. J. Shin, C. Yang and J. H. Oh, Boosting the ambipolar performance of solution-processable polymer semiconductors *via* hybrid side-chain engineering, *J. Am. Chem. Soc.*, 2013, **135**, 9540–9547.

39 W. Li, K. H. Hendriks, A. Furlan, W. C. Roelofs, M. M. Wienk and R. A. Janssen, Universal correlation between fibril width and quantum efficiency in diketopyrrolopyrrole-based polymer solar cells, *J. Am. Chem. Soc.*, 2013, **135**, 18942–18948.

40 W. S. Yoon, S. K. Park, I. Cho, J. A. Oh, J. H. Kim and S. Y. Park, High-Mobility n-Type Organic Transistors Based on a Crystallized Diketopyrrolopyrrole Derivative, *Adv. Funct. Mater.*, 2013, **23**, 3519–3524.

41 Y. Lin, J. Wang, Z. G. Zhang, H. Bai, Y. Li, D. Zhu and X. Zhan, An electron acceptor challenging fullerenes for efficient polymer solar cells, *Adv. Mater.*, 2015, **27**, 1170–1174.

42 W. Jianchang, M. Yuchao, W. Na, L. Yi, L. Jian, W. Lilei and C. Q. Ma, 2,2-Dicyanovinyl-end-capped oligothiophenes as electron acceptor in solution processed bulk heterojunction organic solar cells, *Org. Electron.*, 2015, **23**, 28–38.

43 P. Gautam, R. Misra, E. N. Koukaras, A. Sharma and G. D. Sharma, Donor-acceptor-acceptor-donor small molecules for solution processed bulk heterojunction solar cells, *Org. Electron.*, 2015, **27**, 72–83.

44 P. E. Schwenn, K. Gui, Y. Zhang, P. L. Burn, P. Meredith and B. J. Powell, Kinetics of charge transfer processes in organic solar cells: Implications for the design of acceptor molecules, *Org. Electron.*, 2012, **13**, 2538–2545.

45 Y. Zhong, M. T. Trinh, R. Chen, W. Wang, P. P. Khlyabich, B. Kumar, Q. Xu, C. Nam, M. Y. Sfeir and C. Black, Efficient organic solar cells with helical perylene diimide electron acceptors, *J. Am. Chem. Soc.*, 2014, **136**, 15215–15221.

46 S. H. Liao, H. J. Jhuo, Y. S. Cheng and S. A. Chen, Fullerene Derivative-Doped Zinc Oxide Nanofilm as the Cathode of Inverted Polymer Solar Cells with Low-Bandgap Polymer (PTB7-Th) for High Performance, *Adv. Mater.*, 2013, **25**, 4766–4771.

47 J. W. Jung and W. H. Jo, Low-Bandgap Small Molecules as Non-Fullerene Electron Acceptors Composed of Benzothiadiazole and Diketopyrrolopyrrole for All Organic Solar Cells, *Chem. Mater.*, 2015, **27**, 6038–6043.

48 K. Gui, K. Mutkins, P. E. Schwenn, K. B. Krueger, A. Pivrikas, P. Wolfer, N. S. Stutzmann, P. L. Burn and P. Meredith, A flexible n-type organic semiconductor for optoelectronics, *J. Mater. Chem.*, 2012, **22**, 1800–1806.

49 K. Lin, B. Xie, Z. Wang, R. Xie, Y. Huang, C. Duan, F. Huang and Y. Cao, Star-shaped electron acceptors containing a truxene core for non-fullerene solar cells, *Org. Electron.*, 2017, **52**, 42–50.

50 L. Yang, Y. Chen, S. Chen, T. Dong, W. Deng, L. Lv, S. Yang, H. Yan and H. Huang, Achieving high performance non-fullerene organic solar cells through tuning the numbers of electron deficient building blocks of molecular acceptors, *J. Power Sources*, 2016, **324**, 538–546.

51 J. Pommerehne, H. Vestweber, W. Guss, R. F. Mahrt, B. Auml, H. Bassler, M. Porsch and J. Daub, Efficient two layer leds on a polymer blend basis, *Adv. Mater.*, 1995, **7**, 551–554.

52 Z. G. Zhang, B. Qi, Z. Jin, D. Chi, Z. Qi, Y. Li and J. Wang, Perylene diimides: a thickness-insensitive cathode interlayer for high performance polymer solar cells, *Energy Environ. Sci.*, 2014, **7**, 1966–1973.

53 G. G. Malliaras, J. R. Salem, P. J. Brock and C. Scott, Electrical characteristics and efficiency of single-layer organic light-emitting diodes, *Phys. Rev. B: Condens. Matter Mater. Phys.*, 1998, **58**, 13411–13414.